

NANO EXPRESS

Open Access



Near Infrared-Emitting Cr³⁺/Eu³⁺ Co-doped Zinc Gallogermanate Persistence Luminescent Nanoparticles for Cell Imaging

Qiaojiao Wang^{1,2}, Shuyun Zhang^{1,2}, Zhiwei Li^{1,2} and Qi Zhu^{1,2*}

Abstract

Near infrared (NIR)-emitting persistent luminescent nanoparticles have been developed as potential agents for bioimaging. However, synthesizing uniform nanoparticles with long afterglow for long-term imaging is lacking. Here, we demonstrated the synthesis of spinel structured Zn₃Ga₂Ge₂O₁₀:Cr³⁺ (ZGGO:Cr³⁺) and Zn₃Ga₂Ge₂O₁₀:Cr³⁺,Eu³⁺ (ZGGO:Cr³⁺,Eu³⁺) nanoparticles by a sol-gel method in combination with a subsequent reducing atmosphere-free calcination. The samples were investigated via detailed characterizations by combined techniques of XRD, TEM, STEM, selected area electron diffraction, photoluminescence excitation (PLE)/photoluminescence (PL) spectroscopy, and temperature-dependent PL analysis. The single-crystalline nanoparticles are homogeneous solid solution, possessing uniform cubic shape and lateral size of ~80–100 nm. Upon UV excitation at 273 nm, ZGGO:Cr³⁺,Eu³⁺ exhibited a NIR emission band at 697 nm (²E → ⁴A₂ transition of distorted Cr³⁺ ions in gallogermanate), in the absence of Eu³⁺ emission. NIR persistent luminescence of the sample can last longer than 7200 s and still hold intense intensity. Eu³⁺ incorporation increased the persistent luminescence intensity and the afterglow time of ZGGO:Cr³⁺, but it did not significantly affect the thermal stability. The obtained ZGGO:Cr³⁺,Eu³⁺-NH₂ nanoparticles possessed an excellent imaging capacity for cells in vitro.

Keywords: Near infrared (NIR)-emitting, Persistent luminescent, Bioimaging, Spinel structure, Nanoparticles

Background

Persistent luminescent materials can emit for a long time up to hours after the stoppage of excitation [1]. Mainly due to their great research interests, the phosphors have been commercialized as night or dark environment vision materials for a wide range of applications such as security signs, emergency route signage, identification markers, or medical diagnostics [2]. The typical long-persistent phosphors are the commercialized primary color emitters, such as the red Y₂O₂S:Eu³⁺,Mg²⁺,Ti⁴⁺ or CaS:Eu²⁺,Tm³⁺,Ce³⁺ [3, 4], the green SrAl₂O₄:Eu²⁺,Dy³⁺ or MgAl₂O₄:Mn²⁺ [5, 6], and the blue CaAl₂O₄:Eu²⁺,Nd³⁺ or SrMgSi₂O₆:Eu²⁺,Dy³⁺ [7, 8] phosphors. Although many successes have been made in visible persistent phosphors, the investigation and development

of persistent phosphors in the near infrared (NIR) region (~700–2500 nm) are insufficient. In recent years, the potential applications of persistent phosphors showing red or NIR luminescence have expanded from night-vision security signs to in vivo imaging systems [1, 9, 10].

Persistent luminescent materials with attached photosensitizers as an in vivo agent were firstly tried by Chen and Zhang for photodynamic therapy [11]. Then, Scherman et al. reported a milestone work on in vivo bioimaging with the NIR-emitting phosphor of Ca_{0.2}Zn_{0.9}Mg_{0.9}Si₂O₆:Eu²⁺,Mn²⁺,Dy³⁺ [12]. Soon afterwards, two new NIR-emitting phosphors of CaMgSi₂O₆:Eu²⁺,Mn²⁺,Pr³⁺ and Ca₂Si₅N₈:Eu²⁺,Tm³⁺ with improved performance have been developed by the same group [13, 14]. Recently, Cr³⁺-doped gallate persistent phosphors with NIR emission and long afterglow, including spinel ZnGa₂O₄:Cr³⁺ and their variants, such as Zn₃Ga₂Ge₂O₁₀:Cr³⁺, Zn₃Ga₂GeO₈:Cr³⁺,Yb³⁺,Er³⁺, and ZnGa_{2-x}(Ge/Sn)_xO₄:Cr³⁺, were prepared by a solid-state method [1, 9, 10, 15–21]. The ceramic-disc samples exhibited afterglow time up to 360 h at the NIR region,

* Correspondence: zhuq@smm.neu.edu.cn

¹Key Laboratory for Anisotropy and Texture of Materials (Ministry of Education), Northeastern University, Shenyang, Liaoning 110819, China

²Institute of Ceramics and Powder Metallurgy, School of Materials Science and Engineering, Northeastern University, Shenyang, Liaoning 110819, China

but the bulky materials are unsuitable for in vivo bioimaging. NIR-emitting long-persistent luminescent nanoparticles of $\text{ZnGa}_2\text{O}_4:\text{Cr}^{3+}$ [22, 23], $\text{ZnGa}_2\text{O}_4:\text{Cr}^{3+},\text{Sn}^{4+}$ [19–21], and $\text{Zn}_{2.94}\text{Ga}_{1.96}\text{Ge}_2\text{O}_{10}:\text{Cr}^{3+},\text{Pr}^{3+}$ [9] were synthesized by a sol-gel method in combination with a subsequent reducing atmosphere-free calcination. The persistent luminescence of the nanoparticles powder exhibits bright NIR luminescence in the biological transparency window with a superlong afterglow time. PEGylation greatly improves the biocompatibility and

water solubility of the nanoparticles, which hold great potential for long-term in vivo bioimaging application with high SNR without the need for in situ excitation. It is believed that ions selected from a group consisting of alkaline earth ions, lanthanide ions, and Li^+ co-doping with Cr^{3+} in zinc gallate and zinc gallogermanate would yield remarkable NIR persistent luminescence [1]. Eu^{3+} in oxide hosts always exhibits a red emission at ~ 700 nm arising from the $^5\text{D}_0\text{-}^7\text{F}_4$ intra- $4f$ electronic transition upon short UV excitation into the charge transfer (CT)

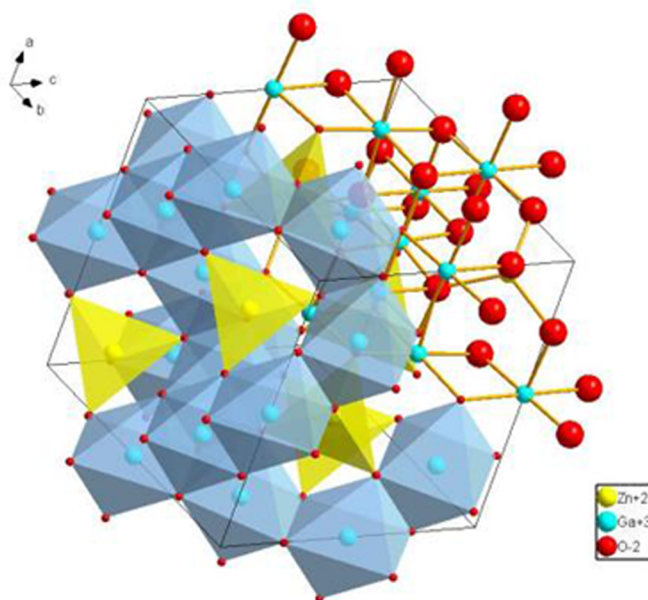
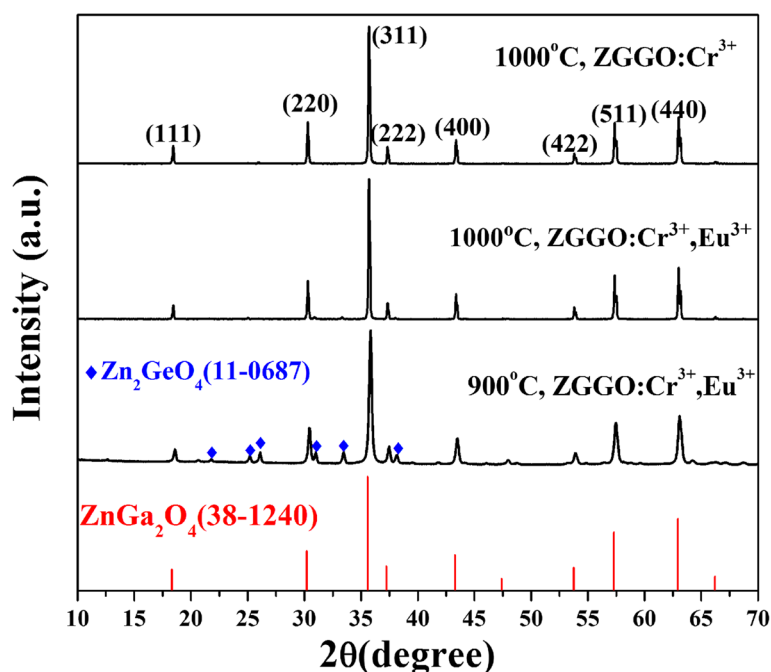


Fig. 1 XRD patterns of the as-prepared $\text{ZGGO}:\text{Cr}^{3+}$ and $\text{ZGGO}:\text{Cr}^{3+},\text{Eu}^{3+}$ and the crystal structure of spinel ZnGa_2O_4

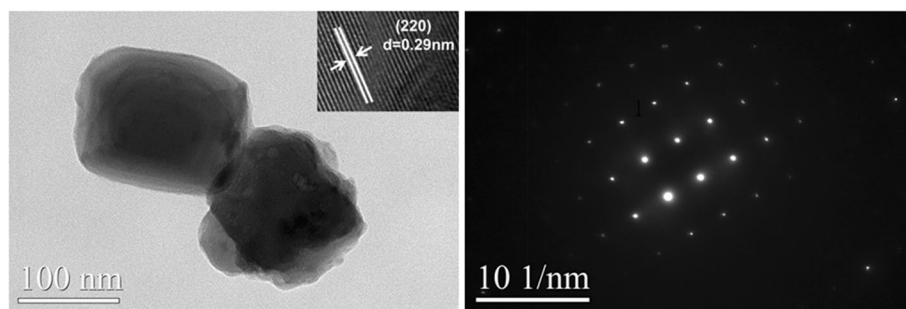


Fig. 2 TEM, HR-TEM (left) image, and SAED pattern (right) of the ZGGO:Cr³⁺,Eu³⁺ nanoparticles

band at 250 nm [24]. On the other hand, Cr³⁺ is a favorable luminescent center in solids because of its narrowband emissions (usually at 700 nm) due to the spin-forbidden ²E-⁴A₂ transition, or a broadband emission (650–1600 nm) due to the spin-allowed ⁴T₂-⁴A₂ transition [1, 20]. In view of these, Cr³⁺/Eu³⁺ co-doped zinc gallate and zinc gallogermanate would yield intense NIR persistent luminescence, owing to that the charge transfer band (CTB) of O²⁻-Eu³⁺ overlaps with the CTB of O²⁻-Ga³⁺, and the emission at ~700 nm from ⁵D₀-⁷F₄ transition of Eu³⁺ overlaps with that from ²E-⁴A₂ transition of Cr³⁺. Furthermore, Eu³⁺ ions substituting for Ga³⁺ ions in distorted octahedral sites may yield suitable host crystal-field strength around Cr³⁺ ions, thus affecting the NIR emission. In this work, Zn₃Ga₂Ge₂O₁₀:Cr³⁺,Eu³⁺ (termed as ZGGO:Cr³⁺,Eu³⁺) nanoparticles were synthesized by a sol-gel method in combination with a subsequent

reducing atmosphere-free calcination, which would be used as the promising nanoprobe for future bioimaging. The samples were investigated via detailed characterizations by combined techniques of X-ray diffractometry (XRD), transmission electron microscopy (TEM), STEM, selected area electron diffraction (SAED), photoluminescence excitation (PLE)/photoluminescence (PL) spectroscopy, and temperature-dependent PL analysis. In the following sections, we report the synthesis, characterization, and application of the ZGGO:Cr³⁺,Eu³⁺ nanoparticles.

Experimental

Synthesis

The starting metal sources are Zn(NO₃)₂·6H₂O, Cr(NO₃)₃·9H₂O, Ga₂O₃, Eu₂O₃, and GeO₂ were all 99.99% pure products purchased from Sinopharm

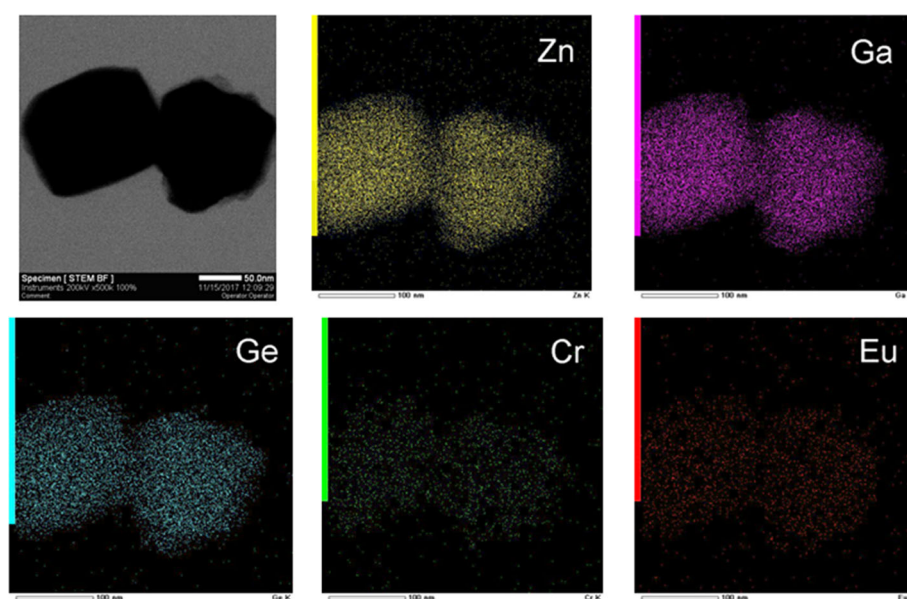


Fig. 3 STEM particle morphology (bright field image, the first picture) and elemental mapping of ZGGO:Cr³⁺,Eu³⁺ nanoparticles

(Shanghai, China). The other reagents are of analytical grade and were purchased from Shenyang Chemical Reagent Factory (Shenyang, China). $\text{Zn}(\text{NO}_3)_2 \cdot 6\text{H}_2\text{O}$ and $\text{Cr}(\text{NO}_3)_3 \cdot 9\text{H}_2\text{O}$ were dissolved in deionized water. Ga_2O_3 and Eu_2O_3 were dissolved in nitric acid solution. GeO_2 and ethylenediaminetetraacetic acid (EDTA) were dissolved in dilute ammonium hydroxide. To the mixture solution, EDTA solution was slowly added without any precipitation, and the molar ratio of total metal ions to EDTA was maintained at 1:2. The atom molar ratio of Zn:Ga:Ge:Cr:Eu was fixed to be 3:1.984:2:0.01:0.006. The final solution was vigorously stirred at room temperature for 1 h, then heated in an oven at 85 °C for the slow evaporation of water until the solution became a sol that finally became a gel. The obtained gel was heated at 200 °C for 3 h to form black porous materials. Finally, the porous materials were ground and annealed under flowing O_2 gas (200 mL/min) at selected temperatures for 2 h.

Surface Functionalization

The $\text{ZGGO:Cr}^{3+}, \text{Eu}^{3+}$ powder was ground for 30 min, then 150 mg of the obtained sample was added into 50 mL of 0.1 mol/L NaOH solution. After sonication for 1 h, the suspension was vigorously stirred for 24 h at room temperature. The resulting colloid solution was centrifuged at 1000 rpm for 10 min to remove large size particles, and the supernatant was centrifuged at 10,000 rpm for 10 min to collect the precipitate. The as-obtained $\text{ZGGO:Cr}^{3+}, \text{Eu}^{3+}\text{-OH}$ nanoparticles were washed with deionized water three times.

Ten milligrams of $\text{ZGGO:Cr}^{3+}, \text{Eu}^{3+}\text{-OH}$ nanoparticles was dispersed in 4 mL of dimethylformamide (DMF) with the assistance of sonication for 10 min. Then, 40 μL of 3-aminopropyl-triethoxysilane (APTES) was added under vigorous stirring for 24 h at room temperature. The as-obtained $\text{ZGGO:Cr}^{3+}, \text{Eu}^{3+}\text{-NH}_2$ nanoparticles

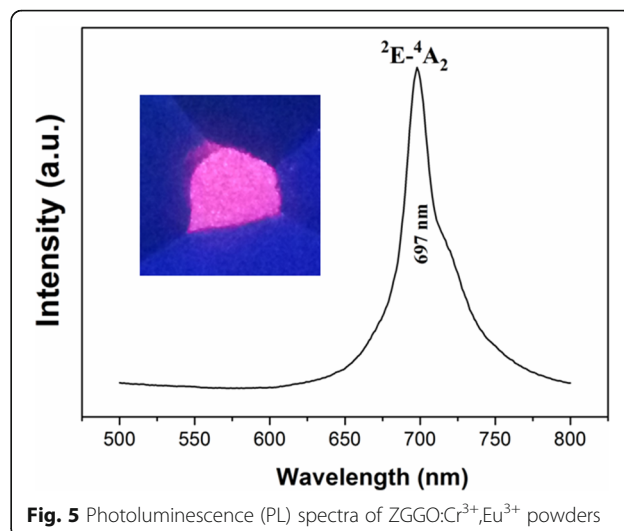


Fig. 5 Photoluminescence (PL) spectra of $\text{ZGGO:Cr}^{3+}, \text{Eu}^{3+}$ powders

were collected by centrifugation at 10,000 rpm for 10 min and washed with DMF three times to remove unreacted APTES.

Cell Imaging

Hek293T cells were cultured in DMEM with 10% FBS and seeded in 35-mm culture dishes for 2 h in a CO_2 incubator. The as-obtained $\text{ZGGO:Cr}^{3+}, \text{Eu}^{3+}\text{-NH}_2$ nanoparticles were dispersed in cell medium (50 mg/mL), which were excited for 10 min by a 254-nm UV lamp and then moved to culture dishes treated for 1 h. After removing the cell medium, 0.1 mL of 1% formaldehyde-PBS was added and the cells were stained with 0.5 mL DAPI dye in the dark for 10 min. Finally, the cells were washed with PBS several times for further characterization.

All studies involving animals were approved by the university animal care and use committee.

Characterization Techniques

Phase identification was performed by XRD (model SmartLab; Rigaku, Tokyo, Japan) operating at 40 kV/40 mA using nickel-filtered $\text{Cu K}\alpha$ radiation and a scanning speed of $6.0^\circ 2\theta/\text{min}$. Morphologies of the products were observed via TEM (model JEM-2000FX; JEOL, Tokyo). Photoluminescence of the phosphors was analyzed with an FP-8600 fluorospectrophotometer (JASCO, Tokyo). The persistent luminescence signals were obtained using Horiba JY FL3-21. The afterglow decay images were recorded in a dark room using a Kodak In-Vivo Imaging System FX Pro. The cell imaging was conducted by a laser scanning confocal microscope (LEICA TCS SP2, Germany).

All studies involving animals were approved by the university animal care and use committee.

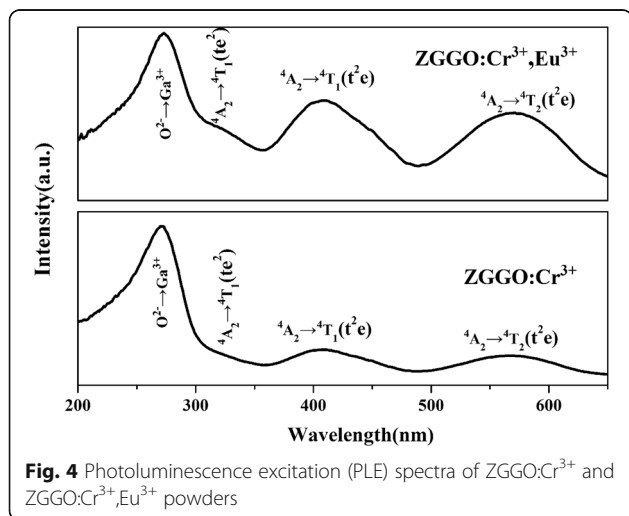


Fig. 4 Photoluminescence excitation (PLE) spectra of ZGGO:Cr^{3+} and $\text{ZGGO:Cr}^{3+}, \text{Eu}^{3+}$ powders

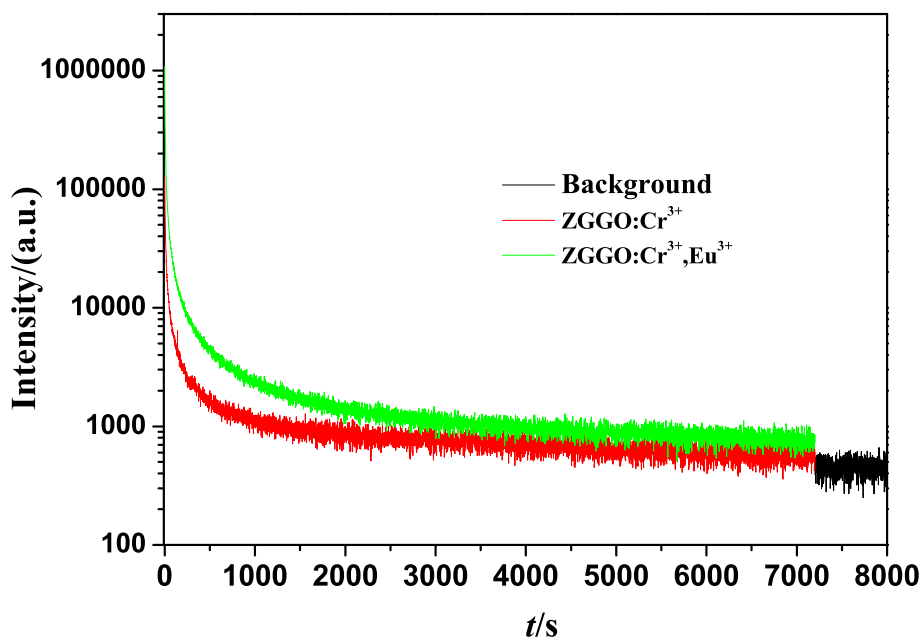


Fig. 6 NIR persistent luminescence decay curves of ZGGO:Cr³⁺ and ZGGO:Cr³⁺,Eu³⁺ powders monitored at 697 nm after 254 nm UV light illumination for 5 min

Results and Discussion

The phase purity of the samples was first investigated by XRD. Figure 1 (up) shows the XRD patterns of the as-prepared ZGGO:Cr³⁺ and ZGGO:Cr³⁺,Eu³⁺ calcined at 1000 °C, which were identified along with the spinel structured Zn₃Ga₂Ge₂O₁₀ [1, 9]. The crystal structure of Zn₃Ga₂Ge₂O₁₀ is the same with that of ZnGa₂O₄ (JCPDS No. 38-1240), which is the solid solution of ZnGa₂O₄ and Zn₂GeO₄. In the structure of Zn₃Ga₂Ge₂O₁₀, Ge plays the role of substitution of Ga,

conducive to the formation of traps, while ZnGa₂O₄ is the dominant crystal structure [1]. There are two kinds of cations in one-unit cell; Zn²⁺ and Ga³⁺ are surrounded by four and six oxygen anions forming a tetrahedron and an octahedron, respectively (Fig. 1, below). Calculations from the diffraction data yielding the cell constants for ZGGO:Cr³⁺ are $a = b = \sim 0.8335$ nm, close to that of spinel ZnGa₂O₄ ($a = b = \sim 0.8335$ nm, JCPDS No. 38-1240). Due to the larger ionic radii of Eu³⁺ (for sixfold coordination, $r_{\text{Eu}^{3+}} = 0.0947$ nm and $r_{\text{Ga}^{3+}} = 0.062$ nm) [25], a larger value of $a = b = \sim 0.8336$ nm was observed for ZGGO:Cr³⁺,Eu³⁺. Profile broadening analysis of the (311) Bragg reflection was conducted by applying the Scherrer equation for average crystallite sizes of 83 ± 6 nm for ZGGO:Cr³⁺ and ZGGO:Cr³⁺,Eu³⁺ samples. In Fig. 1 (up), we also find that the resulting products calcined at 900 °C are the mixture of spinel phase (JCPDS No. 38-1240) and rhombohedral one (JCPDS No. 11-0687), indicating a calcination temperature of ≥ 1000 °C is needed for yielding spinel Zn₃Ga₂Ge₂O₁₀ in a phase pure form.

Figure 2 (left) shows the TEM morphology for ZGGO:Cr³⁺,Eu³⁺ particles, clearly indicating that they entirely consist of cubic particles, with lateral sizes of ~ 80 – 100 nm. The sharp corners and the well-resolved lattice fringes suggest their excellent crystallinity, while the spacings of ~ 0.29 nm correspond well to the (220) plain of spinel structured ZnGa₂O₄ ($d(220) = \sim 0.29$ nm, JCPDS No. 38-1240) (inset in Fig. 2). Because the

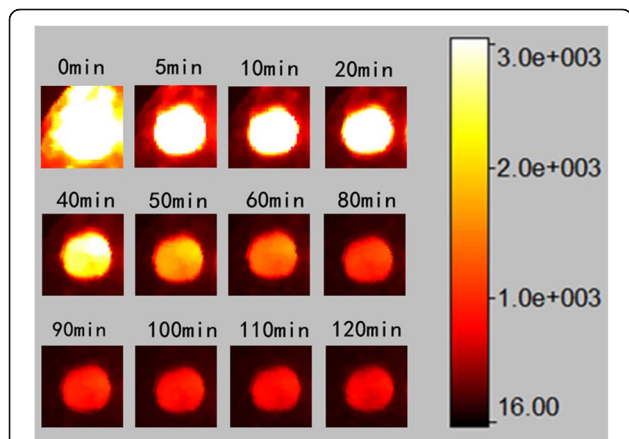


Fig. 7 NIR afterglow decay images of ZGGO:Cr³⁺,Eu³⁺ powders obtained by a Kodak In-Vivo Imaging System FX Pro at different times after stopping UV irradiation

particle sizes are close to the average crystallite sizes calculated from the XRD data, the obtained samples may be single crystalline. The SAED analysis (Fig. 2 (right)) further confirmed that the nanoparticles under analysis are of single crystalline. The nanoparticles investigated here are direct solid-state solutions rather than a mechanical mixture. Elemental mapping of Zn, Ga, Ge, Cr, and Eu provides evidence of this solid solution, as

revealed in Fig. 3 for ZGGO:Cr³⁺,Eu³⁺. Not only does each particle contain Zn, Ga, Ge, Cr, and Eu, but all elements are evenly distributed among the particles.

Figure 4 shows the excitation spectra of the ZGGO:Cr³⁺ and ZGGO:Cr³⁺,Eu³⁺ powder at room temperature. The excitation spectrum monitored at 697 nm covers a very broad spectral region (from 200 to 650 nm) and consists of four main excitation bands

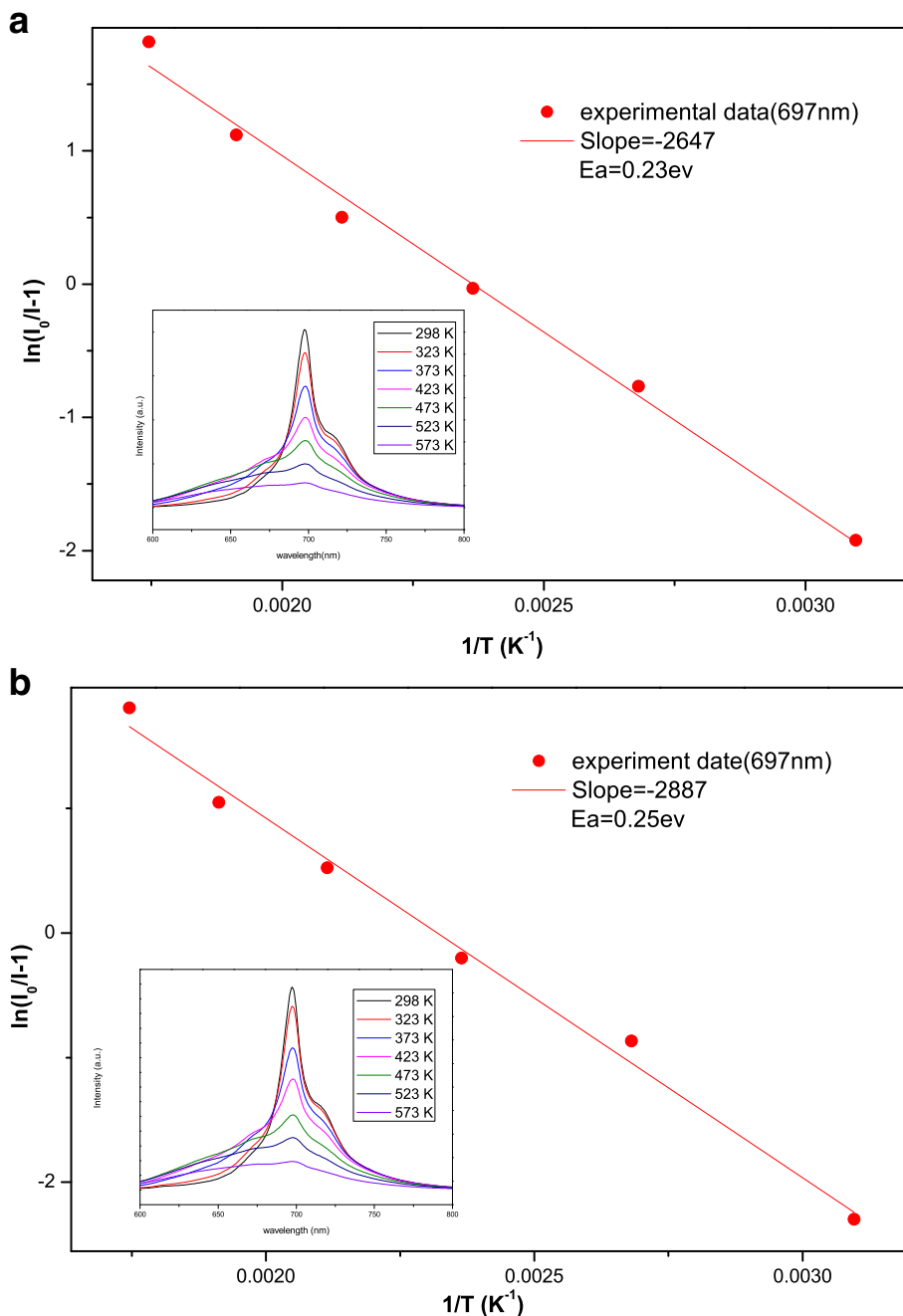


Fig. 8 Activation energy of thermal quenching for emission bands in **a** ZGGO:Cr³⁺ and **b** ZGGO:Cr³⁺,Eu³⁺ powders. The insets show the corresponding temperature dependence of PL spectra from 298 to 573 K

peaking at 273, 328, 410, and 569 nm, respectively. The excitation band at 273 nm is ascribed to the charge transfer band of $O^{2-}-Ga^{3+}$ in $ZnGa_2O_4$ host, while the later bands originate from the inner transitions of Cr^{3+} , including the 328-nm band originating from the ${}^4A_2 \rightarrow {}^4T_1(t^2e)$ transition, the 410-nm band originating from the ${}^4A_2 \rightarrow {}^4T_1(t^2e)$, and the 569-nm band originating from the ${}^4A_2 \rightarrow {}^4T_2(t^2e)$ [19, 20]. Incorporation of Eu^{3+} did not appreciably alter the positions of the PLE bands but significantly increased the intensities of the inner transitions of Cr^{3+} , with I_{410}/I_{273} increasing from 0.18 to 0.56. The above results indicate that Eu^{3+} incorporation is conducive to the visible light excitation. However, the strongest excitation band at 273 nm also revealed that the charge transfer band of $O^{2-}-Ga^{3+}$ is the most effective excitation wavelength. Excitation of the powder at 273 nm gave a NIR emission band at 697 nm (Fig. 5) due to the ${}^2E \rightarrow {}^4A_2$ transition in distorted Cr^{3+} ions in gallogermanate, in the absence of Eu^{3+} emission.

The NIR persistent luminescence decay curves of $ZGGO:Cr^{3+}$ and $ZGGO:Cr^{3+},Eu^{3+}$ nanoparticles were monitored at 697 nm after 254 nm UV light illumination (xenon lamp as the light source) for 5 min at room temperature as shown in Fig. 6. The result demonstrates that the NIR persistent luminescence of the $ZGGO:Cr^{3+}$ sample can last longer than 7200 s and still hold appreciable intensity. The persistent luminescence intensity of $ZGGO:Cr^{3+},Eu^{3+}$ increases with the incorporation of Eu^{3+} ion. It is believed that lanthanide ions co-doping with Cr^{3+} in zinc gallogermanate would yield remarkable NIR persistent luminescence, because of its important role in increasing the amount of anti-site defects which is the responsible for persistent luminescence of Cr^{3+} in zinc gallogermanate host [1]. On the other hand, NIR persistent luminescence of $ZGGO:Cr^{3+},Eu^{3+}$ sample can last longer than that of $ZGGO:Cr^{3+}$, indicating that Eu^{3+} incorporation can increase the afterglow time. Figure 7 shows NIR afterglow decay images of $ZGGO:Cr^{3+},Eu^{3+}$ powders obtained by a Kodak In-Vivo Imaging System FX Pro at different times after stopping UV irradiation, further confirming that the afterglow can last longer than 120 min and keep an intense NIR emission intensity.

For evaluating the performance of phosphor application, especially for high-power applications, thermal stability is a key parameter. To evaluate the thermal quenching behavior of the phosphors in this work, the PL spectra were analyzed at temperatures ranging from 298 to 573 K (Fig. 8). For all samples, elevating the temperature yielded a decrease in the emission intensities at 697 nm. To obtain a more comprehensive picture of the thermal quenching behavior and estimate the value of its activation energy (E_a), the

Arrhenius equation (Eq. (1)) was employed as follows [26–28]:

$$I_T = \frac{I_0}{1 + c \exp\left(-\frac{E_a}{kT}\right)} \quad (1)$$

where I_0 and I_T are the intensities of the initial and final temperatures, respectively; c is the rate constant; E_a is the activation energy; and k is the Boltzmann constant (8.629×10^{-5} eV K^{-1}). Figure 8 shows the $\ln(I_0 / I_T - 1)$ vs $10,000 / T$ relationship lines for the emission band centered at 697 nm for $ZGGO:Cr^{3+}$ and $ZGGO:Cr^{3+},Eu^{3+}$. Similar activation energies were calculated: $E_a = 0.23$ eV for $ZGGO:Cr^{3+}$ and $E_a = 0.25$ eV for $ZGGO:Cr^{3+},Eu^{3+}$. The probability that a nonradiative transition occurs per unit time (α) can be defined according to Eq. (2) as follows [29]:

$$\alpha = s \exp\left(-\frac{E_a}{kT}\right) \quad (2)$$

where s is the frequency factor (s^{-1}), k is the Boltzmann constant, and T is the temperature. It can be seen that a lower activation energy (E_a) leads to a greater probability (α) of a nonradiative transition. Because of the similar activation energy, $ZGGO:Cr^{3+}$ and $ZGGO:Cr^{3+},Eu^{3+}$ exhibited closed thermal stability, indicating Eu^{3+} incorporation did not significantly affect the thermal stability. However, associated phonon side bands (PSBs) centered at 670 nm became dominant at a higher temperature, thus inducing enhanced emission peaks.

We also investigated the PL excitation and emission spectra of the aqueous dispersion of $ZGGO:Cr^{3+},Eu^{3+}$ (Fig. 9). Compared to the $ZGGO:Cr^{3+},Eu^{3+}$ powder, the

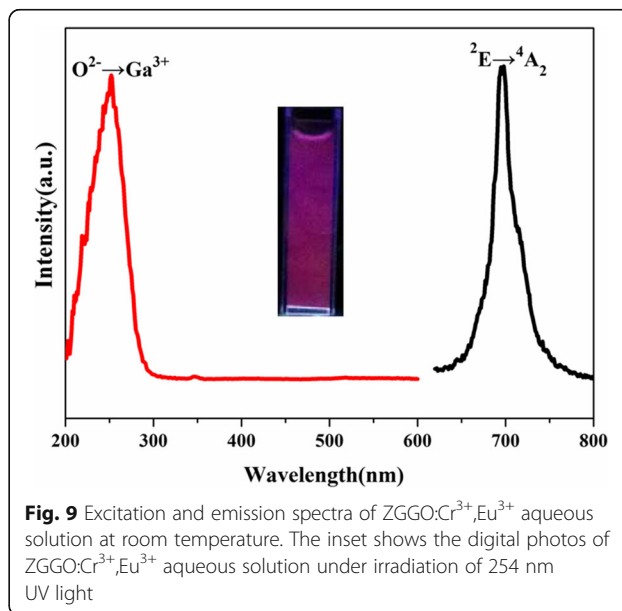


Fig. 9 Excitation and emission spectra of $ZGGO:Cr^{3+},Eu^{3+}$ aqueous solution at room temperature. The inset shows the digital photos of $ZGGO:Cr^{3+},Eu^{3+}$ aqueous solution under irradiation of 254 nm UV light

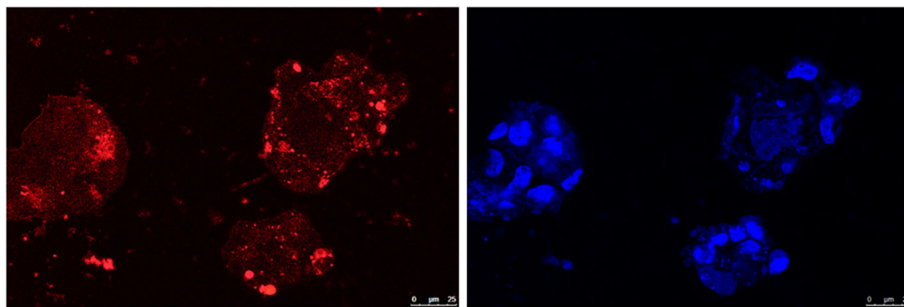


Fig. 10 LSCM image (left, red color) of Hek293T cells incubated with ZGGO:Cr³⁺,Eu³⁺-NH₂ nanoparticles for 1 h. The right image (blue color) is appearance of the same cells stained with 0.5 mL DAPI dye. Scale bar = 25 μm

aqueous dispersion exhibited almost the same profile of the PL excitation and emission curves except the relatively weak excitation intensity at 300 and 600 nm. The weakened intensity is probably due to the quenching effect of the O–H vibration of water.

Hek293T cells were employed here for in vitro imaging test. The as-obtained ZGGO:Cr³⁺,Eu³⁺-NH₂ nanoparticles were dispersed in cell medium (50 mg/mL), which were excited for 10 min by a 254-nm UV lamp and then moved to culture dishes treated for 1 h. Figure 10 (left, red color) shows the cell luminescence imaging collected on a laser scanning confocal microscope in the absence of excitation. The afterglow luminescence signal of the Hek293T cells was still strong enough to be precisely measured after 1 h, though the afterglow luminescence signals gradually decreased over time. For comparison, the cell luminescence imaging was collected on a laser scanning confocal microscope by another mode from the same cells stained with 0.5 mL DAPI dye (right in Fig. 10, simultaneous excitation). The similar imaging signals suggested that the ZGGO:Cr³⁺,Eu³⁺-NH₂ nanoparticles possessed an excellent imaging capacity for cells in vitro.

Conclusions

In this work, spinel structured ZGGO:Cr³⁺ and ZGGO:Cr³⁺,Eu³⁺ nanoparticles were synthesized by a sol-gel method in combination with a subsequent reducing atmosphere-free calcinations. The samples were investigated via detailed characterizations by combined techniques of XRD, TEM, STEM, SAED, PLE/PL spectroscopy, and temperature-dependent PL analysis. The nanoparticles with uniform cubic shape and lateral size of ~80–100 nm are of single crystalline and homogeneous solid solution. Excitation of the powder at 273 nm gave a NIR emission band at 697 nm due to the ²E → ⁴A₂ transition in distorted Cr³⁺ ions in gallogermanate, in the absence of Eu³⁺ emission. NIR persistent luminescence of the ZGGO:Cr³⁺,Eu³⁺ can last longer than 7200 s and still hold intense intensity. The persistent

luminescence intensity of ZGGO:Cr³⁺ and the afterglow time increase with the incorporation of Eu³⁺ ion. However, Eu³⁺ incorporation did not significantly affect the thermal stability. Finally, the as-obtained ZGGO:Cr³⁺,Eu³⁺-NH₂ nanoparticles possessed an excellent imaging capacity for cells in vitro.

Funding

This work was supported in part by the Fundamental Research Funds for the Central Universities (Grant N160204008) and the National Training Program of Innovation and Entrepreneurship for undergraduates (201710145115).

Availability of Data and Materials

Not applicable

Authors' Contributions

QQW, SYZ, and ZWL carried out the experiments. QZ and QQW were involved in the results discussion and drafted the manuscript. All the authors have read and approved the final manuscript.

Competing Interests

The authors declare that they have no competing interests.

Publisher's Note

Springer Nature remains neutral with regard to jurisdictional claims in published maps and institutional affiliations.

Received: 18 January 2018 Accepted: 14 February 2018

Published online: 27 February 2018

References

- Pan Z, Lu YY, Liu F (2012) Sunlight-activated long-persistent luminescence in the near-infrared from Cr³⁺-doped zinc gallogermanates. *Nat Mater* 11: 58–63
- Yen WM, Shionoya S, Yamamoto H (2006) Practical applications of phosphors. CRC, Boca Raton
- Ye S, Zhang J, Zhang X, Lu S, Ren X, Wang XJ (2007) Mn²⁺ activated red phosphorescence in BaMg₂Si₂O₇: Mn²⁺, Eu²⁺, Dy³⁺ through persistent energy transfer. *J Appl Phys* 101:063545
- Jia D (2006) Enhancement of long-persistence by Ce co-doping in CaS: Eu²⁺, Tm³⁺ red phosphor. *J Electrochem Soc* 153(11):H198–H201
- Matsuzawa T, Aoki Y, Takeuchi N, Murayama Y (1996) New long phosphorescent phosphor with high brightness, SrAl₂O₄:Eu²⁺,Dy³⁺. *J Electrochem Soc* 143(8):2670–2673
- Wang XJ, Jia DD, Yen WM (2003) Mn²⁺ activated green, yellow, and red long persistent phosphors. *J Lumin* 102:34–37
- Aitasalo T, Holsa J, Jungner H, Lastusaari M, Niittykoski J (2001) Mechanisms of persistent luminescence in Eu²⁺, RE³⁺ doped alkaline earth aluminates. *J Lumin* 94:59–63

8. Lin YH, Tang ZL, Zhang ZT, Wang XX, Zhang JY (2001) Preparation of a new long afterglow blue-emitting $\text{Sr}_2\text{MgSi}_2\text{O}_7$ -based photoluminescent phosphor. *J Mater Sci Lett* 20(16):1505–1506
9. Abdulkayum A, Chen JT, Zhao Q, Yan XP (2013) Functional near infrared-emitting $\text{Ce}^{3+}/\text{Pr}^{3+}$ co-doped zinc gallogermanate persistent luminescent nanoparticles with superlong afterglow for in vivo targeted bioimaging. *J Am Chem Soc* 135:14125–14133
10. Ogawa M, Regino CAS, Choyke PL, Kobayashi H (2009) In vivo target-specific activatable near-infrared optical labeling of humanized monoclonal antibodies. *Mol Cancer Ther* 8:232–239
11. Chen W, Zhang J (2006) Using nanoparticles to enable simultaneous radiation and photodynamic therapies for cancer treatment. *J Nanosci Nanotechnol* 6:1159–1166
12. le Masne de Chermont Q, Chaneac C, Seguin J, Pelle F, Maitrejean S, Jolivet JP, Gourier D, Bessodes M, Scherman D (2007) Nanoprobes with near-infrared persistent luminescence for in vivo imaging. *Proc Natl Acad Sci U S A* 104:9266
13. Maldiney T, Leconte A, Viana B, Bessière A, Bessodes M, Gourier D, Richard C, Scherman D (2011) Controlling electron trap depth to enhance optical properties of persistent luminescence nanoparticles for in vivo imaging. *J Am Chem Soc* 133:11810
14. Maldiney T, Kaikkonen MU, Seguin J, le Masne de Chermont Q, Bessodes M, Airene KJ, Yla-Herttuala S, Scherman D, Richard C (2012) In vivo optical imaging with rare earth doped $\text{Ca}_2\text{Si}_5\text{N}_8$ persistent luminescence nanoparticles. *Opt Mater Express* 2:261–268
15. Duan XL, Liu J, Wu YC, Yu FP, Wang XQ (2014) Structure and luminescent properties of $\text{Co}^{2+}/\text{Cr}^{3+}$ co-doped ZnGa_2O_4 nanoparticles. *J Lumin* 153:361–368
16. Zhao HX, Yang CX, Yan XP (2016) Fabrication and bioconjugation of B-III and Cr-III co-doped ZnGa_2O_4 persistent luminescent nanoparticles for dual-targeted cancer bioimaging. *Nano* 8:18987–18994
17. Liu F, Liang Y, Pan Z (2014) Detection of up-converted persistent luminescence in the near infrared emitted by the $\text{Zn}_3\text{Ga}_2\text{GeO}_8:\text{Ce}^{3+}, \text{Yb}^{3+}, \text{Er}^{3+}$ phosphor. *Phys Rev Lett* 113:177401
18. Allix M, Chenu S, Veron E, Poumeyrol T, Kouadri-Boudjethia EA, Alahrache S, Porcher F, Massiot D, Fayon F (2013) Considerable improvement of long-persistent luminescence in germanium and tin substituted ZnGa_2O_4 . *Chem Mater* 25:1600–1606
19. Zou R, Huang J, Shi JP, Huang L, Zhang X, Wong KL, Zhang HW, Jin D, Wang J, Su Q (2017) Magnetic-NIR persistent luminescent dual-modal $\text{ZGOCS@MSNs@Gd}_2\text{O}_3$ core-shell nanoprobes for in vivo imaging. *Chem Mater* 29:3938–3946
20. Zou R, Gong SM, Shi JP, Jiao J, Wong KL, Zhang HW, Wang J, Su Q (2017) Silica shell-assisted synthetic route for mono-disperse persistent nanophosphors with enhanced in vivo recharged near-infrared persistent luminescence. *Nano Res* 10:2070–2082
21. Zhou W, Zou R, Yang X, Huang N, Huang J, Liang H, Wang J (2015) Core-decomposition-facilitated fabrication of hollow rare-earth silicate nanowalnuts from core-shell structures via the Kirkendall effect. *Nano* 7:13715–13722
22. Maldiney T, Bessière A, Seguin J, Teston E, Sharama SK, Viana B, Bos AJJ, Dorenbos P, Bessodes M, Gourier D, Scherman D, Richard C (2014) The in vivo activation of persistent nanophosphors for optical imaging of vascularization, tumours and grafted cells. *Nat Mater* 13:418–426
23. Li Z, Zhang Y, Wu X, Huang L, Li D, Fan W, Han G (2015) Direct aqueous-phase synthesis of sub-10 nm "luminous pearls" with enhanced in vivo renewable near-infrared persistent luminescence. *J Am Chem Soc* 137:5304–5307
24. Zhu Q, Xiong M, Li JG, Liu WG, Wang ZH, Li XD, Sun XD (2015) $(\text{Y,Tb,Eu})_2\text{O}_3$ monospheres for highly fluorescent films and transparent hybrid films of color tunable emission. *RSC Adv* 5:36122–36128
25. Shannon RD (1976) Revised effective ionic radii and systematic study of inter atomic distances in halides and chalcogenides. *Acta Cryst* 32:751–767
26. Zhang NM, Guo CF, Zheng JM, Su XY, Zhao J (2014) Synthesis, electronic structures and luminescent properties of Eu^{3+} doped KGdTiO_4 . *J Mater Chem C* 2:3988–3994
27. Lee SP, Chan TS, Chen TM (2015) Novel reddish-orange-emitting $\text{BaLa}_2\text{Si}_2\text{S}_8:\text{Eu}^{2+}$ thiosilicate phosphor for LED lighting. *ACS Appl Mater Interfaces* 7:40–44
28. Xia ZG, Zhou J, Mao ZY (2013) Near UV-pumped green-emitting $\text{Na}_3(\text{Y,Sc})\text{Si}_3\text{O}_9:\text{Eu}^{2+}$ phosphor for white-emitting diodes. *J Mater Chem C* 1:5917–5924
29. Lv WZ, Jia YC, Zhao Q, Jiao MM, Shao BQ, Lu W, You HP (2014) Crystal structure and luminescence properties of $\text{Ca}_8\text{Mg}_3\text{Al}_2\text{Si}_7\text{O}_{28}:\text{Eu}^{2+}$ for WLEDs. *Adv Opt Mater* 2:183–188

Submit your manuscript to a SpringerOpen® journal and benefit from:

- Convenient online submission
- Rigorous peer review
- Open access: articles freely available online
- High visibility within the field
- Retaining the copyright to your article

Submit your next manuscript at ► springeropen.com
